Robustness evaluation of split ring resonator antenna system for wireless brain care in semi-anatomical ellipsoid head model

Robustness Evaluation of Split Ring Resonator Antenna System for Wireless Brain Care in Semi-Anatomical Ellipsoid Head Model

Shubin Ma, Leena Ukkonen, Lauri Sydänheimo, Toni Björninen

BioMediTech Institute and Faculty of Biomedical Sciences and Engineering
Tampere University of Technology
Tampere, Finland
{shubin.ma, leena.ukkonen, lauri.sydanheimo, toni.bjorninen}@tut.fi

Abstract ─ Robustness evaluation is a critical part to verify the applicability of wireless implantable devices. In this work, we present a semi-anatomical ellipsoid head model to evaluate the robustness of a split ring resonator inspired antenna system toward variable implant location, tissue layer thicknesses, and antenna orientation with respect to the human head. The system consists of a passive wearable part placed on the scalp and a cortical implant that carries a passive UHF RFID microsystem. According to our results, the antenna system is robust toward variability: it enables the remote powering of a −18 dBm RFID microsystem at distance between 0.5 and 1.1 meter at various locations and orientations with respect to the head and for skull thickness up to 1 cm.

Index Terms ─ Antennas, brain modelling, implantable biomedical devices, RFID, robustness.

I. INTRODUCTION

With more than 86 billion neurons and other supportive glial cells constituting the cerebrum, the brainstem and the cerebellum, the human brain forms the central nervous system that regulates all our daily physiological activities. Thus, any injury to the brain usually leads to serious deterioration of physical and mental capacity. In the pursue toward better life quality for those suffering from debilitating neurological conditions, researchers have recently found wireless brain care based on implantable sensors and stimulators a compelling approach to achieve a long term intracranial physiological monitoring, prosthesis controlling and treatment for neurological disorders [1-3].

Among the wireless modalities for the data transfer, modulated backscattering or RFID-inspired approaches are compelling as they offer low-power data communications that is pertinent to battery-free implants [4-6]. To establish effective far field communications with a cortical backscattering implant, we have recently proposed a spatially distributed split-ring resonator inspired antenna system composed of a small, thin and flexible implantable part that couples to a head-worn part acting as a performance booster [7]. Human body is an extremely complex operation environment for antennas, and thus computational electromagnetics and appropriate human body models are indispensable in the assessment of the electromagnetic performance of implantable and wearable antennas. In the aforementioned work, due to the difficulty of building a multiple-layer head phantom in practice, we used a simple homogenous block model to conduct the first feasibility evaluation of our antenna system and obtained a good agreement between the simulation and experimental results. That model included an average estimation for the dielectric properties of the human head, but due to its simplified geometry, it cannot be used to predict the impact of variation of the tissue layer thickness or radiation properties of the antenna system at different locations on the head or when its orientation with respect to the head changes. In practice, these are all crucial aspects, as the location of the implant varies according to the application and its exact orientation is hard to control during surgery. Thus, the antenna system must be robust toward these factors. It must also remain functional under anatomical variability since the tissue layer thicknesses are different for different individuals. Consequently, computational modelling of the human head with more details is pertinent to verify the applicability of the antenna system.

Currently, high-resolution medical imaging based computational models offer the most detailed structural information for computational modelling. However, for this reason they are not only computationally heavy, but reflect the anatomical details of a certain scanned individual with no possibility for adjusting the tissue layer thickness to assess the impact of anatomical variability. To overcome these limitations and to achieve holistic robustness evaluation of our system, we present modelling results obtained from a semi-anatomical human head model, which we have built by integrating a seven-layer ellipsoid with the anatomical head model of an adult male. Meanwhile, various electromagnetic CAD tools based on various numerical methods are available to provide extremely good accuracy [8]. In this journal, we chose Ansys HFSS 17.0 to conduct the simulation and analysis.

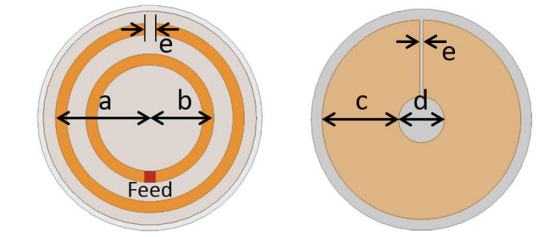

Geometrical parameter (mm)	a	b	c	d	e
	8.6	5.7	20.8	12.6	1.0

Fig. 1. Antenna system with its geometrical dimensions.

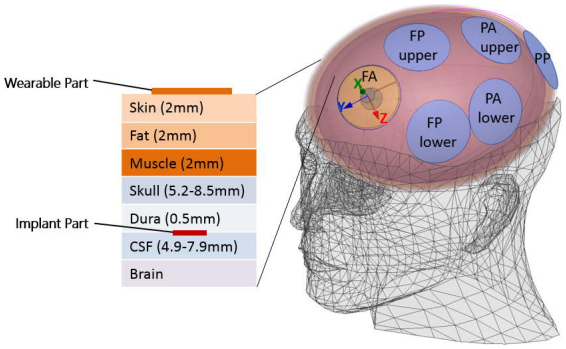

Fig. 2. Semi-anatomical human head model with the layered ellipsoid.

II. SIMULATION SETUP

A. Antenna System

The antenna system is based on the split ring resonator structure with an implantable and wearable parts. Fig. 1 shows the antenna structure and its geometrical dimensions. The implant part provides the self complex-conjugate matching with the IC that is connected to feed point in Fig. 1. The fully passive wearable part is for antenna gain improvement [7]. The cross-sectional view in Fig. 2 shows its implementation in intracranial environment. We assume the implant to be affixed to the dura, which is a tough fibrous membrane that forms the sack enclosing the subarachnoid space (SAS) and that wearable part is concentrically placed on the scalp. We use 35 µm thick copper as the conductor for the antenna system and the substrates for the wearable and implant parts are 2 mm thick EPDM (Ethylene-Propylene-Diene-Monomer) (ε_r=1.26, tanδ=0.007 at 915 MHz) and 50 µm thick flexible polyethylene (ε_r=2.25, tanδ=0.001 at 915 MHz), respectively. The coating material for the implant part is 1 mm thick silicone (ε_r=2.2, tanδ=0.007 at 915 MHz). The RFID microchip in the simulation is modelled by the parallel connection of the resistance and capacitance of 2.85 kΩ and 0.91 pF, respectively [9].

B. Antenna Performance Indicators

In the antenna development for passive RFID tags, the attainable read range (d_{tag}) between the tag and the off-body reader is one of the most important performance indicators. Friis' transmission equation can be used to estimate d_{tag} as

$$d_{tag} = \frac{\lambda}{4\pi}\sqrt{\frac{De_r\tau EIRP}{P_{ic0}}}, \qquad (1)$$

where the d_{tag} is in inverse proportion to RFID IC wake-up power (P_{ic0}) and proportional to antenna directivity (D), radiation efficiency (e_r), power transfer efficiency (τ), and the equivalent isotropically radiated power limitation ($EIRP$). The power transfer efficiency defined in (2) measures the portion of the power delivered from the antenna to the IC relative to the maximum power available from the antenna. It is given by

$$\tau = \frac{4\mathrm{Re}(Z_A)\mathrm{Re}(Z_c)}{|Z_A+Z_C|^2} \qquad (2)$$

where Z_A and Z_C are the antenna and IC impedances, respectively. In other words, $0 < \tau \leq 1$ quantifies the goodness of the complex conjugate impedance matching between the antenna and the IC.

Among all the five variables shown in (1), except for P_{ic0} and $EIRP$, which are fixed by the IC design and the regional wireless communication regulatory committee, other parameters can be optimized to maximize d_{tag}. Therefore, in this work we will focus on the analysis of D, e_r and τ in the semi-anatomical human head model.

C. Semi-anatomical Head Model

We built the semi-anatomical human head model by integrating a seven-layer ellipsoid with the ANSYS anatomical human head model. The seven layers of the ellipsoid were constructed as ellipsoid shells with an adjustable thicknesses representing skin, fat, muscle, skull, dura, CSF (cerebrospinal fluid) and brain (grey matter). To model the relative permittivity and the electromagnetic energy dissipation in the biological matter, we used the four-term Cole-Cole relaxation model introduced in [10]. The loss model accounts for both loss sources: polarizability and ohmic loss due to conduction current. All the model parameters are available in [11] and Table 1 lists the dielectric

Table 1: Dielectric properties of human Tissues at 950 MHz.

Tissue	ε_r	σ (S/m)
Skin	41.405	0.867
Fat (not infiltrated)	5.462	0.051
Muscle	55.032	0.943
Skull (cancellous)	20.788	0.340
Dura	44.426	0.961
CSF	68.638	2.413
Brain (grey matter)	52.725	0.942

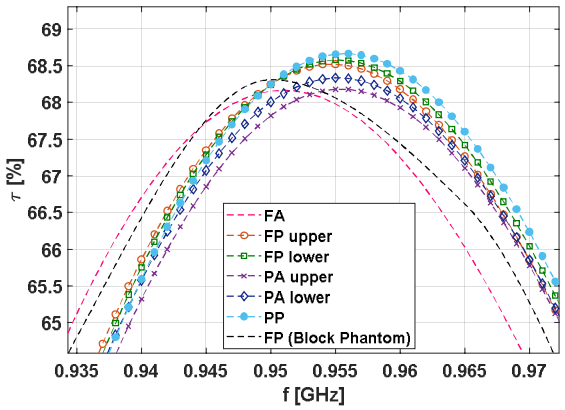

Fig. 3. Simulated power transfer efficiency in the semi-anatomical head model and the block phantom model.

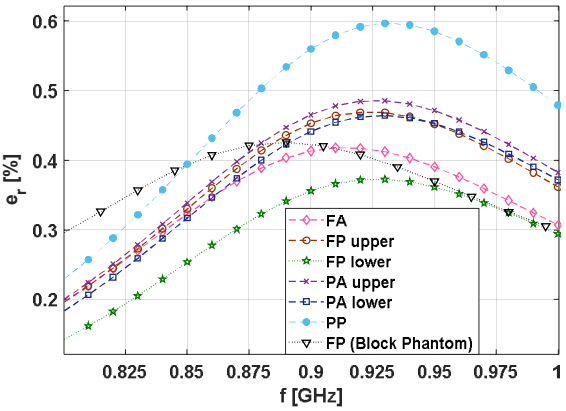

Fig. 4. Simulated antenna radiation efficiency in the semi-anatomical head model and the block phantom model.

properties of each tissue type at 950 MHz.

Fig. 2 illustrates the semi-anatomical head model and six different placements of the antenna system in four different regions: the frontal anterior (FA), frontal posterior (FP) with upper and lower positions, parietal anterior (PA) with upper and lower positons and parietal posterior (PP). At each location, we defined the nominal antenna orientation such that a line drawn through the middle of the split gap in the wearable part intersects the minor axis of the ellipsoid pointing along the person's height.

The thicknesses of skin, fat, and muscle tissue layers are almost independent of the positions on the head and thus we set a fixed value of 2 mm for each layer in this model [12]. The thickness of dura layer also varies over small range from 0.3 mm to 0.8 mm [13] and therefore we fixed the thickness of this layer to 0.5 mm. However, the thicknesses of the skull and the cerebrospinal fluid (CSF) layers vary greatly depending on the location. Hence, we measured these values over several cross-sectional slices of the anatomical head model to obtain averaged values. The thinner regions of the skull tend to coincide with wider SAS. Moreover, since we consider affixing the implant to the dura, the range for the skull thickness we present in Fig. 2 is the mean minimum thickness over the cross-sections, whereas the CSF layer thickness is the mean maximum SAS width. This selection was made, because we consider its benefit for both safety and wireless performance to maximize/minimize the distance between the implant and the cortex/wearable part.

Table 2: Tissue thickness in different location [mm]

Tissue \ Position	FA	FP	PA	PP
Skin	2	2	2	2
Fat	2	2	2	2
Muscle	2	2	2	2
Skull	5.2	4.0	3.9	8.5
Dura	0.5	0.5	0.5	0.5
CSF	6.1	7.2	7.9	4.9

Table 2 lists the thickness of each tissue layer within the four regions we have considered in our model. In order to model the antenna at a specific region, we have assigned the corresponding layer thicknesses over the whole ellipsoid. However, since the separation between the implant and wearable part (and the material composition at this location) is dominant for the system's performance, we expect the thickness variations at other regions to have comparatively negligible impact on it.

III. RESULTS AND DISCUSSION

ANSYS HFSS uses the finite element method (FEM) to generate the electromagnetic field solutions. To obtain a high-level accuracy, the mesh size needs to be small enough. HFSS uses iterative process to refine the mesh by minimizing the change in the solution between consecutive iterations. In HFSS, the default parameter to evaluate the convergence of the solution of a problem with a single excitation port is the S-parameter magnitude. Typically, it converges before the far field parameters. Therefore, in this work, we monitored the expression cache of τ, D and e_r in each iteration to ensure the accuracy and reliability of the results. In the last iteration of the mesh refinement, all these parameters were changing less than 0.07%.

For comparison, we also modelled the antenna system in a seven-layer block phantom with a surface area of 30×30 cm^2. The layer thicknesses in the block phantom were identical to those in semi-anatomical model. Here the brain layer thickness was set to 7.5 cm so that the total thickness of the block was 25.2 cm. In our previous work, we have shown thorough experiments in liquid phantom [7] that the antenna system is robust toward moderately large rotational and translational misalignments between the wearable and implant parts [7] and thus we omit this analysis here.

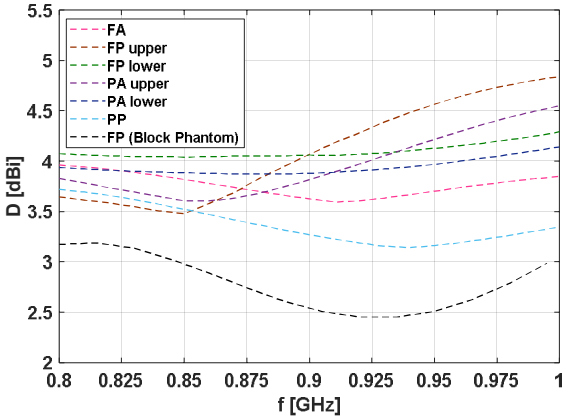

Fig. 5. Simulated antenna directivity in the semi-anatomical head model and the block phantom model.

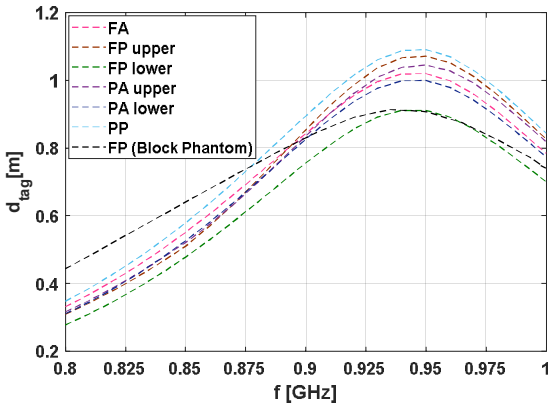

Fig. 6. Simulated maximum attainable read range in the semi-anatomical head model and the block phantom model.

A. Impact of Antenna Location

To facilitate the implementation of the wearable part on the curved surface of the ellipsoid, we flattened the contact surface between the two locally. However, since the curvature radius is large in comparison with the size of the wearable part, we expect this to introduce minimal impact on the results. In order to evaluate the impact of the antenna location on its electromagnetic performance judiciously, we first set the thickness for each layer of the head model to the values from the FP position. In this way, we can isolate the impact of the location (different curvature radii and impact of the anatomical part of the model) from the impact of variable tissue layer thicknesses. For comparison, we performed the same simulation in the layered block model with identical layer thicknesses.

Fig. 3 shows the simulated power transfer efficiency with different implant locations. The results verify that the implant position has negligible impact on τ. This is because only the dielectric properties of tissue types closest to the antenna are determinant for its impedance. For the same reason, the result from the block phantom, shown with the black dashed line, also matches closely with those from the semi-anatomical model. This implies that the simple block phantom model is adequate for initial antenna impedance tuning.

Fig. 4 shows the antenna radiation efficiency with different implant locations. The location causes a clear level shift in the radiation efficiency, but does not change its peak frequency. Generally, the highest efficiency occurs in PP region, with the peak value of 0.60% at 925 MHz. The lowest efficiency occurs in the FP region at the lower location with its maximum value of 0.38%. The result from the block phantom model lies close to the mean value of those from the semi-anatomical model, but there is a difference in the frequency of the peak value, which shifts to 880 MHz in the block model.

As shown in Fig. 5, the antenna directivity varies up to 1.5 dB between the different implant locations. In comparison, the block phantom model underestimates it over the whole frequency range. Overall, we conclude that although 1.5 dB maximum variation in D between the six locations is clearly noticeable, it is relatively smaller than that observed in the radiation efficiency (Fig. 4).

Fig. 6 shows the attainable read range computed from equation (1) with the simulated quantities from the

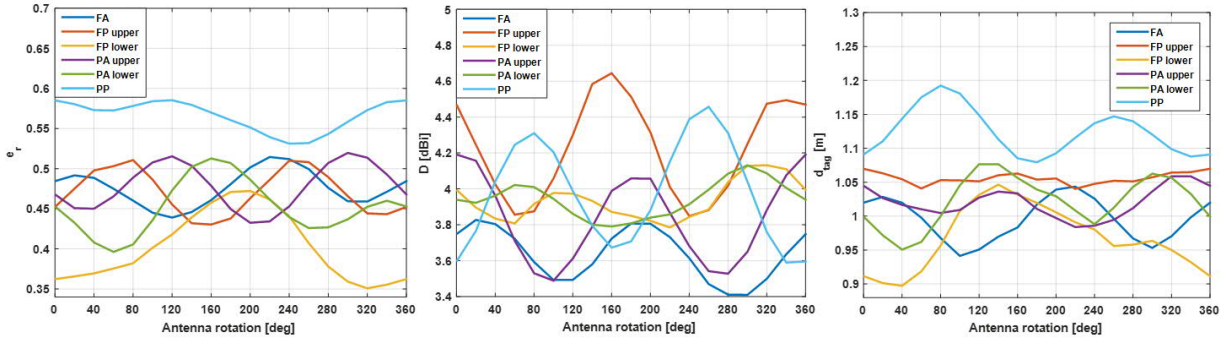

Fig. 7. Simulated results at six implant locations in the antenna rotation test

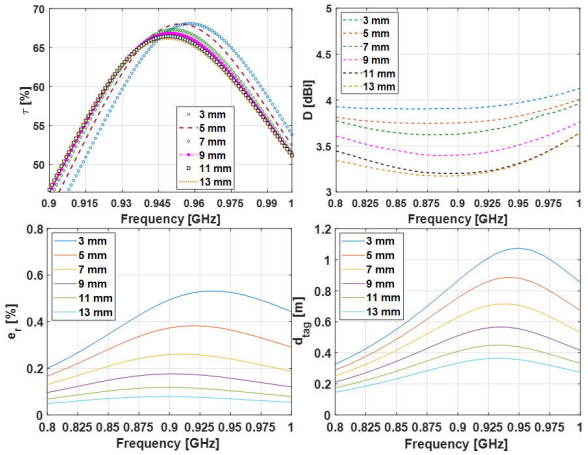

Fig. 8. Simulated results with the continuous change in the thickness of skull layer.

six locations and the block phantom. The peak value of d_{tag} varies from 0.9 m to 1.1 m around the frequency 930 MHz. Here the peak value of the result from the block phantom is close to the minimum of those from the semi-anatomical model.

In general, the implant location has relatively larger influence on D and e_r and very little impact on τ. Nonetheless, the antenna shows robustness toward the location in the semi-anatomical model: the peak value of attainable read range varies only ±10 cm around 1 meter with no shift in the center frequency of the peak value.

B. Impact of Antenna Orientation

Due to the structure limitation of the block phantom model, it cannot be expected to predict the correct relationship between the antenna orientation and its electromagnetic performance. This information is valuable for evaluating the antenna feasibility in the real implementation where the orientation of the implant part

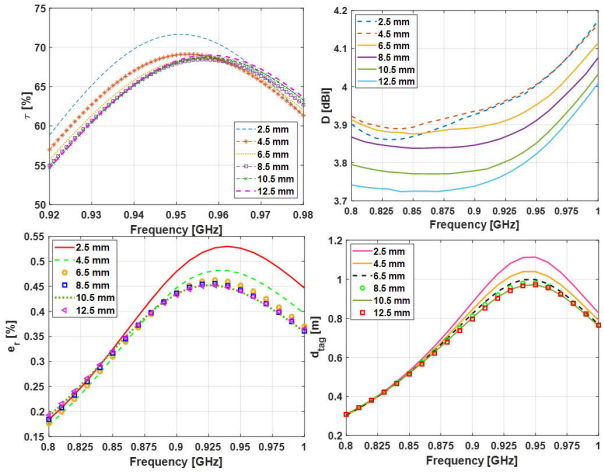

Fig. 9. Simulated results with the continuous change in the thickness of CSF layer.

is difficult to control. Therefore, we modelled the antenna system in the semi-anatomical model at the previously discussed six locations with a clockwise rotation around the x-axis with a step of 20 degrees at the frequency of 950 MHz. According to the simulated results shown in Fig. 7, the rotation of the antenna introduces a periodically varying fluctuating response in e_r and D versus the rotation angle, but overall the magnitude of the fluctuation remains below 10 %. Consequently, the attainable read range remains between 0.9 meter and 1.2 meters implying that the impact of the rotation is similar in magnitude as the impact of the location discussed above.

C. Impact of Variable CSF and Skull Thickness

To assess the impact of anatomical variability, we changed the thickness of the two most variable tissue layers; skull and CSF stepwise over intervals that cover the ranges shown in Fig. 2 and discussed in Section II.C. First, we set all the layer thickness to the values from the PA lower location (see Table II) and then increased the thickness of the skull from 3 mm to 13 mm with a step of 2 mm. According to the results shown in Fig. 8, D, e_r and d_{tag} decrease notably with the increase in the skull thickness. When the thickness is above 1 cm, the attainable read range drops below 0.5 m. The reason behind this is that the increase in the separation between the implant and wearable part weakens the electromagnetic coupling between the two.

A similar test was conducted for the CSF layer by changing its thickness from 2.5 mm to 12.5 mm with a step of 2 mm while the other layer thicknesses were fixed. Fig. 9 presents the simulated results. The decreasing trend in D with increasing layer thickness is similar to that observed in the case of the skull. However, overall the change is smaller. Likewise, the change in e_r versus the layer thickness shows similar character as in the case of skull thickness. However, here the separation (and therefore the coupling) between the implant and wearable parts remains constant and correspondingly the change in e_r is smaller and contributed to the increase in the amount of the high-conductivity CSF in the proximity of the antenna which increases the ohmic loss. Overall, the attainable read range remained at approximately 1 meter as the CSF layer thickness reached 12.5 mm.

VI. CONCLUSION

We evaluated the robustness of a spatially distributed implantable antenna system carrying an RFID microsystem toward several sources of variability that are likely to occur in practice. To achieve this, we used a semi-anatomical human head model based on a layered ellipsoid to mimic the human head environment with freely adjustable tissue layer thickness. The antenna system provided approximately consistent performance

at six different locations covering most of antenna placements on the head and insensitivity toward antenna orientation with respect to the head. Moreover, the attainable read range of the implanted RFID remained above 0.5 m with the thickness of the skull reaching 1 cm. These results ensure the feasibility of our antenna system as a wireless platform in brain care applications further.

Our ongoing and future work focuses on integrating physiological sensors into the evaluated antenna system and development of a wearable part that provides circular polarization.

ACKNOWLEDGMENT

This research was funded by Academy of Finland, Jane and Aatos Erkko Foundation.

REFERENCES

[1] Ryan M. Neely, David K. Piech, Samantha R. Santacruz, Michel M. Maharbiz and Jose M. Carmena, "Recent advances in neural dust: toward a neural interface platform," *Current Opin. Neurobiol.*, vol. 50, pp. 64–71, 2018.

[2] M. W. A. Khan, L. Sydänheimo, L. Ukkonen and T. Björninen, "Inductively powered pressure sensing system integrating a far-field data transmitter for monitoring of intracranial pressure," *IEEE Sensors J.*, vol. 17, no. 7, pp. 2191–2197, 2017.

[3] M. J. Cook, T. J. O'Brien, S. F. Berkovic et al., "Prediction of seizure likelihood with a long-term, implanted seizure advisory system in patients with drug-resistant epilepsy: A first-in-man study," *Lancet Neurol.*, vol. 12, no. 6, pp. 563–571, 2013.

[4] E. Kampianakis, A. Sharma, J. Arenas and M. S. Reynolds, "A dual-band wireless power transfer and backscatter communication approach for implantable neuroprosthetic devices," *2017 IEEE International Conference on RFID (RFID)*, Phoenix, AZ, 2017, pp. 67-72.

[5] C. W. L. Lee, A. Kiourti and J. L. Volakis, "Miniaturized fully passive brain implant for wireless neuropotential acquisition," *IEEE Antennas and Wireless Propagation Letters*, vol. 16, pp. 645-648, 2017.

[6] H. N. Schwerdt, F. A. Miranda and J. Chae, "Wireless fully passive multichannel recording of neuropotentials using photo-activated RF backscattering methods," *IEEE Transactions on Microwave Theory and Techniques*, vol. 63, no. 9, pp. 2965-2970, 2015.

[7] Shubin Ma, L. Ukkonen, L. Sydänheimo and T. Björninen, "Split ring resonator antenna system with implantable and wearable parts for far field readable backscattering implants," Proc. IEEE AP Soc. Intl. Symp. on Antennas and Propag., 2017, San Diego, CA, USA, pp. 1689–1690.

[8] Vandenbosch, G. A. E., "State-of-the-art in antenna software benchmarking: Are we there yet?" IEEE Antenna and Propagation Magazine, vol. 56, No. 4, August 2014.

[9] T. Björninen, L. Sydänheimo and L. Ukkonen, "Development and validation of an equivalent circuit model for UHF RFID IC based on wireless tag measurements," *AMTA Symp.*, 2012, Bellevue, WA, USA, pp. 6.

[10] S Gabriel, R W Lau and C Gabriel, "The dielectric properties of biological tissues: III. Parametric models for the dielectric spectrum of tissues," *Phys. Med. Biol.*, vol. 41, no. 11, pp. 2271–2293, 1996.

[11] IT'IS Foundation, Tissue Properties [Online]. Available: https://www.itis.ethz.ch/virtual-population/tissue-properties/downloads

[12] A. Drossos, V. Santomaa and N. Kuster, "The dependence of electromagnetic energy absorption upon human head tissue composition in the frequency range of 300-3000 MHz," *IEEE Trans. Microwave Theory Techn.*, vol. 48, no. 11, pp. 1988–1995, 2000.

[13] A. Bashkatov, E. Genina, Y. Sinichkin, V. Kochubey, N. Lakodina and V. Tuchin, "Glucose and mannitol diffusion in human dura Mater," *Biophysical J.*, vol. 85, no. 5, pp. 3310–3318, 2003

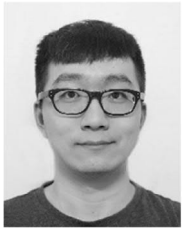

Shubin Ma received the B.E. degree in communication engineering from Xi'an University of Posts and Telecommunications, China, in 2011 and the M.Sc. (tech.) degree from Tampere University of Technology, Finland, in 2017.

He is currently pursuing the Ph.D. degree with the BioMediTech Institute and Faculty of Biomedical Science and Engineering at Tampere University of Technology. His research interests include electromagnetic modelling, antenna designs, and implantable biomedical systems.

Lauri Sydänheimo received the M.Sc. and Ph.D. degrees in electrical engineering from the Tampere University of Technology (TUT), Tampere, Finland. He is currently a Professor with the Faculty of Biomedical Sciences and Engineering, TUT.

He has authored more than 200 publications in radio-frequency identification tag and reader antenna design and wireless system performance improvement. His current research interests include wireless data communication and wireless identification and sensing.

Leena Ukkonen received the M.Sc. and Ph.D. degrees in electrical engineering from the Tampere University of Technology (TUT), Tampere, Finland, in 2003 and 2006, respectively.

She is currently a Professor and Academy Research Fellow with the Faculty of Biomedical Science and Engineering, TUT, Tampere, where she is leading the Wireless Identification and Sensing Systems Research Group.

Toni Björninen received the M.Sc. and doctoral degrees in Electrical Engineering in 2009 and 2012, respectively, from Tampere University of Technology (TUT), Tampere, Finland.

He is currently an Academy of Finland Research Fellow in BioMediTech Institute and Faculty of Biomedical Sciences and Engineering in TUT. He has been a Visiting Postdoctoral Scholar in Berkeley Wireless Research Center in UC Berkeley and in Microwave and Antenna Institute in Electronic Engineering Dept., Tsinghua University, Beijing. His research focuses on technology for wireless health including implantable and wearable antennas and sensors, and RFID-inspired wireless solutions.

Dr. Björninen is an author of more than 140 peer-reviewed scientific publications. He is a Senior Member of IEEE and serves as an Associate Editor in IET Electronics Letters and IEEE Journal of Radio Frequency Identification.